

1 **Small molecule cognitive enhancer reverses age-related memory decline in mice.**

2
3 **SHORT TITLE: Reversing aging related deficits**

4
5 **Authors:** Karen Krukowski^{1,2}, Amber Nolan^{2,3,*}, Elma S. Frias^{1,2,*}, Morgane Boone^{4*},
6 Gonzalo Ureta⁵, Katherine Grue^{1,2}, Maria-Serena Paladini^{1,2}, Edward Elizarraras^{1,2}, Luz
7 Delgado⁵, Sebastian Bernales⁵, Peter Walter^{4,6} and Susanna Rosi^{1,2,7,8,9}

8
9 ¹ Department of Physical Therapy and Rehabilitation Science, University of California at
10 San Francisco, San Francisco, CA, USA.

11 ² Brain and Spinal Injury Center, University of California at San Francisco, San
12 Francisco, CA, USA.

13 ³ Department of Pathology, University of California at San Francisco, San Francisco,
14 CA, USA.

15 ⁴ Biochemistry and Biophysics, University of California at San Francisco, San Francisco
16 CA, USA.

17 ⁵ Fundación Ciencia & Vida, Santiago, Chile.

18 ⁶ Howard Hughes Medical Institute, University of California at San Francisco, San
19 Francisco, CA, USA.

20 ⁷ Department of Neurological Surgery, University of California at San Francisco, San
21 Francisco, CA, USA.

22 ⁸ Weill Institute for Neuroscience, University of California at San Francisco, San
23 Francisco, CA, USA.

24 ⁹ Kavli Institute of Fundamental Neuroscience, University of California at San Francisco,
25 San Francisco, CA, USA.

26
27 *authors contributed equally

28 **Corresponding Authors:**

29
30 Susanna Rosi, Ph.D. Lewis and Ruth Cozen Chair II

31 Professor

32 1001 Potrero Ave,

33 Zuckerberg San Francisco General Hospital

34 Building #1 Room 101

35 San Francisco, CA 94110

36 Tel.: +1-415-206-3708

37 Email: susanna.rosi@ucsf.edu

38
39 Peter Walter, PhD, Professor

40 Box 2200, UCSF

41 San Francisco, CA 94143

42 Phone: +1-415-476-5017

43 Email: peter@walterlab.ucsf.edu

45 **ONE SENTENCE SUMMARY**

46 Inhibition of the integrated stress response restores neuronal and immune dysfunction
47 and alleviates memory deficits in aged mice.

48

49 **ABSTRACT**

50 With increased life expectancy age-associated cognitive decline becomes a growing
51 concern, even in the absence of recognizable neurodegenerative disease. The
52 integrated stress response (ISR) is activated during aging and contributes to age-
53 related brain phenotypes. We demonstrate that treatment with the drug-like small-
54 molecule ISR inhibitor ISRIB reverses ISR activation in the brain, as indicated by
55 decreased levels of activating transcription factor 4 (ATF4) and phosphorylated
56 eukaryotic translation initiation factor eIF2. Furthermore, ISRIB treatment reverses
57 spatial memory deficits and ameliorates working memory in old mice. At the cellular
58 level in the hippocampus, ISR inhibition i) rescues intrinsic neuronal electrophysiological
59 properties, ii) restores spine density and iii) reduces immune profiles, specifically
60 interferon and T cell-mediated responses. Thus, pharmacological interference with the
61 ISR emerges as a promising intervention strategy for combating age-related cognitive
62 decline in otherwise healthy individuals.

63

64 **INTRODUCTION**

65

66 “Of the capacities that people hope will remain intact as they get older, perhaps the
67 most treasured is to stay mentally sharp” (1).

68

69 The impact of age on cognitive performance represents an important quality-of-life and
70 societal concern, especially given our prolonged life expectancy. While often discussed
71 in the context of disease, decreases in executive function as well as learning and
72 memory decrements in older, healthy individuals are common (2, 3, 4, 5). According to

73 the US Department of Commerce the aging population is estimated by 2050 to reach
74 83.7 million individuals above 65 years of age in the US; this represents a rapidly
75 growing healthcare and economic concern (6).

76

77 Age-related decline in memory has been recapitulated in preclinical studies with old
78 rodents (7-10). Specifically, prior studies have identified deficits in spatial memory (9,
79 11), working and episodic memory (8, 10) and recognition memory (12), when
80 comparing young, adult mice with older sex-matched animals. The hippocampus is the
81 brain region associated with learning and memory formation and is particularly
82 vulnerable to age-related changes in humans and rodents (13-16). Deficits in a number
83 of cellular processes have been suggested as underlying causes based on correlative
84 evidence, including protein synthesis (17), metabolism (18), inflammation (19), and
85 immune responses (9, 11, 20, 21). While providing a wealth of parameters to assess, by
86 and large the causal molecular underpinnings of age-related memory decline have
87 remained unclear.

88

89 The principle that blocking protein synthesis prevents long-term memory storage was
90 discovered many years ago (22). With age there is a marked decline of protein
91 synthesis in the brain that correlates with defects in proper protein folding (12, 23-25).
92 Accumulation of misfolded proteins can activate the integrated stress response (ISR)
93 (26), an evolutionary conserved pathway that decreases protein synthesis. In this way,
94 the ISR may have a causative role in age-related cognitive decline. We previously
95 discovered that interference with the drug-like small-molecule inhibitor (integrated stress

96 response inhibitor, or ISRIB) rescued traumatic brain injury-induced behavioral and
97 cognitive deficits (27-29), suggesting that this pharmacological tool may be useful in
98 testing this notion.

99

100 Increasing age leads to structural and functional changes in hippocampal neurons.
101 Specifically, in old animals there is an increase in neuronal hyperpolarization after
102 spiking activity (“afterhyperpolarization”, or AHP) that decreases intrinsic neuronal
103 excitability and correlates with memory deficits (13-16, 30). Aging also manifests itself
104 with synaptic excitability changes in the hippocampus that correlate with a reduction in
105 the bulbous membrane projections that form the postsynaptic specializations of
106 excitatory synapses, termed dendritic spines (31, 32). Morphological changes in
107 dendritic spine density are critical for spatial learning and memory (33, 34). Whether
108 these age-related neuronal changes can be modified or are linked with ISR activation
109 has yet to be determined.

110

111 In addition to neuronal changes, ISR activation can modify immune responses via
112 alterations in cytokine production (35). Indeed, maladaptive immune responses have
113 been linked with cognitive decline in the old brain (8, 9, 11, 20). Initial studies focused
114 on age-associated cytokine responses, including interferon (IFN)-mediated cognitive
115 changes (20, 36). Type-I IFN responses can induce age-related phenotypes in rodents.
116 Furthermore, the adaptive immune system (T cell infiltration into the old brain) can
117 regulate neuronal function via IFN- γ production (21), suggesting the possibility that age-
118 induced maladaptive immune responses and the ISR are linked. Here we explore the

119 possibility of ISR inhibition by ISRIB as a potential strategy for modifying age-induced
120 neuronal, immune, and cognitive dysfunction.

121

122

123 **RESULTS**

124

125 *ISRIB resets the ISR in the brain of old mice.*

126

127 ISR activation leads to global reduction in protein synthesis but also to translational up-
128 regulation of a select subset of mRNAs whose translation is controlled by small
129 upstream open-reading frames in their 5'-UTRs (37, 38). One well-studied ISR-
130 upregulated target protein is ATF4 (activating transcription factor 4) (39, 40). We
131 recently showed ISRIB administration reversed mild head trauma-induced elevation in
132 ATF4 protein (28). Using the same ISRIB treatment paradigm of daily injections on 3
133 consecutive days (27, 28), we found decreased age-associated ATF4 protein levels in
134 mouse brain lysates when compared to vehicle-treated controls during ISRIB
135 administration (**Supplemental Figure 1**). ATF4 levels 18 days after cessation of ISRIB
136 treatment showed persistent reduction in age-induced ATF4 protein levels that were
137 indistinguishable from young mice (**Figure 1A, B, Supplemental Figure 2A**).

138

139 The key regulatory step in the ISR lies in the phosphorylation of eukaryotic translation
140 initiation factor eIF2 (26). Four known kinases can phosphorylate Ser51 in its α -subunit
141 of (eIF2 α) to activate the ISR (41): HRI (heme-regulated inhibitor), PKR (double-

142 stranded RNA-dependent protein kinase), PERK (PKR-like ER kinase) and GCN2
143 (General amino acid control nonderepressible 2). Only three of these kinases are known
144 to be expressed in the mammalian brain (PKR, PERK, GCN2). To understand upstream
145 modifiers of age-related ISR activation, we investigated the impact of age and ISRIB
146 administration on the expression of these kinases. We found a modest, but significant
147 increase in activated GCN2 (as indicated by its phosphorylated form p-GCN2) when
148 comparing young and old brain lysates (**Figure 1C, Supplemental Figure 2B**).
149 Moreover, when ISRIB was administered weeks prior (**Figure 1A**), GCN2 activation
150 returned to levels comparable to young brains (**Figure 1C, Supplemental Figure 2B**).
151 Age and ISRIB did not impact phosphorylation status of PERK and PKR in total brain
152 lysates (**Figure 1D,E, Supplemental Figure 2B**). Thus, brief ISRIB administration in
153 the old brain has long-lasting effects on ISR activation.

154

155 *Inhibition of the ISR reverses age-induced decline in spatial learning and memory.*

156

157 To assess whether the reduction in ISR activation affects age-related cognitive defects,
158 we tested the capacity for spatial learning and memory in young and old mice in a radial
159 arm water maze (27, 42). This particular forced-swim behavior tool measures
160 hippocampal-dependent spatial memory functions in rodents and has been previously
161 used to assess age-related cognitive deficits (7, 43). Animals were trained for two days
162 (two learning blocks/day) to locate a platform hidden under opaque water in one of the
163 eight arms using navigational cues set in the room (**Figure 2A**). We recorded the total
164 number of entries into the non-target arm (errors) before the animal found the escape

165 platform with automated tracking software and used it as a metric of learning. After two
166 days of training, young animals averaged one error prior to successfully locating the
167 escape platform, while old animals averaged three errors, indicating their reduced
168 learning capacity (**Supplemental Figure 3A**).

169

170 We next tested whether pharmacological inhibition of the ISR could modify the age-
171 related spatial learning deficits. ISRIB treatment started the day before the first training
172 day and continued with daily injections throughout the duration of the training (3
173 injections in total; see **Figure 2A**, left). By the end of two days of training, ISRIB-treated
174 old animals averaged two errors prior to finding the escape platform, while vehicle-
175 treated old animals averaged three, denoting significant learning improvement in the
176 mice that received ISRIB (**Supplemental Figure 3B**). No difference in learning
177 performance was measured in young mice that received the identical treatment
178 paradigm (**Supplemental Figure 3C**), suggesting that ISRIB-induced learning
179 improvement measured in this training regime is age-dependent. These results were
180 confirmed in an independent old animal cohort, in which we tested an additional ISR
181 inhibitor (Cmp-003, a small molecule with improved solubility and pharmacological
182 properties (PCT/US18/65555)), using an identical training/injection paradigm
183 (**Supplemental Figure 3D**). Old animals that received Cmp-003 made significantly
184 fewer errors prior to locating the escape platform than old animals that received vehicle
185 injections, again indicating significant learning improvement.

186

187 Spatial memory of the escape location was measured one week later by reintroducing
188 the animals into the pool and measuring the number of errors before they located the
189 hidden platform. The animals did not receive any additional treatment during this task.
190 Old mice treated with ISRIB one week before made significantly fewer errors compared
191 to matched, vehicle-treated old male (**Figure 2B**) and female (**Supplemental Figure 4**)
192 mice. Remarkably, the memory performance of old animals treated with ISRIB a week
193 before was comparable to that of young mice (**Figure 2B**). These results demonstrate
194 that brief treatment with ISRIB rescues age-induced spatial learning and memory
195 deficits, cementing a causative role of the ISR on long-term memory dysfunction .

196

197

198 *ISRIB administration improves age-induced deficits in working and episodic memory*
199 *weeks after treatment.*

200

201 Given the long-lasting effect of brief ISRIB treatment on ATF4 protein levels in the brain
202 and on memory function one week after drug administration, we next tested the duration
203 of ISRIB effects on age-related cognitive function. On experimental day 20 (18 days
204 post ISRIB treatment, **Figure 2A**, right), we measured working and episodic memory
205 using a delayed-matching-to-place paradigm (DMP) (27, 44) in the same animal cohort
206 without additional ISRIB treatment. Previous work has demonstrated that old mice
207 display significant impairments when compared to young mice (8, 10). During DMP
208 animals learned to locate an escape tunnel attached to one of 40 holes in a circular
209 table using visual cues. The escape location was changed daily, forcing the animal to

210 relearn its location. To quantify performance, we used analysis tracking software to
211 measure “escape latency”, reporting the time taken by the mouse to enter the escape
212 tunnel.

213

214 Old mice that received ISRIB treatment 18 days earlier displayed significant
215 improvement over the four-day testing period (**Figure 2C**; Day 20 vs. Day 23). By Day
216 23 post-treatment animals were locating the escape tunnel on average 20 seconds
217 faster than the matched-vehicle group (**Figure 2C**). This behavior is indicative of
218 improved working and episodic memory. By contrast, old animals that received vehicle
219 injections did not learn the task (**Figure 2C**; Day 20 vs. Day 23), as previously observed
220 (8, 10). These results demonstrate that ISRIB administration increases cognitive
221 performance in a behavioral paradigm measured weeks after administration.

222

223 *ISRIB treatment reverses age-associated changes in hippocampal neuron function.*

224

225 To determine the neurophysiological correlates of ISRIB treatment on cognition, we
226 investigated its effects on hippocampal neuronal function. Utilizing whole cell patch
227 clamping, we recorded intrinsic electrophysiological firing properties and synaptic input
228 in CA1 pyramidal neurons of young and old mice and compared them to those of old
229 mice treated with a single injection of ISRIB the day prior to recording (**Figure 3A**).

230

231 We evaluated alterations in intrinsic excitability by measuring action potential shape and
232 frequency properties and passive membrane response properties produced by a series

233 of hyperpolarizing and depolarizing current steps (20 steps from -250 to 700 pA, 250 ms
234 duration). We also assessed the hyperpolarization of the membrane potential following
235 high frequency firing, specifically the AHP following ~50 Hz spiking activity induced with
236 a current step (**Figure 3A**). In agreement with previous reports (13-16, 30), old mice
237 displayed a significantly increased AHP amplitude when compared to young mice
238 (**Figure 3B**). ISRIB treatment reversed the age-induced increase in AHP amplitude,
239 rendering the CA1 neuronal response in ISRIB-treated old mice indistinguishable from
240 young mice (**Figure 3B**). We did not find significant differences in other action potential
241 or passive membrane properties between groups (**Supplemental Figure 5**).

242

243 We also measured spontaneous excitatory postsynaptic currents (sEPSC), while
244 holding the cell at -75 mV in a voltage clamp. Both the frequency and amplitude of
245 sEPSCs were indistinguishable between groups (**Supplemental Figure 6**). These data
246 support that ISRIB treatment in old animals restores neuronal function to levels
247 comparable to young neurons by affecting intrinsic excitability and specifically reducing
248 the AHP following high frequency firing.

249

250 *ISRIB treatment reduces dendritic spine loss.*

251

252 To determine if ISRIB might affect age-induced synaptic structural changes, we
253 quantified dendritic spine density after ISRIB treatment in old mice with fluorescently
254 labeled excitatory neurons (marked by a genomically encoded Thy1-YFP fusion
255 protein). The hippocampus of old mice is characterized by a reduction in dendritic spine
256 density that correlates with diminished cognitive output (31, 32). Old Thy1-YFP

257 expressing mice received ISRIB treatment and two days of behavioral training as
258 described in **Figure 2A**. At the end of Day 2, we terminated the animals and harvested
259 the brains for quantification of dendritic spine density in the hippocampus (stratum
260 radiatum of CA1) (**Figure 3C**) using confocal microscopy imaging and unbiased
261 analysis (**Figure 3D**). Similar to previous reports, we measured a significant reduction in
262 dendritic spine density in old when compared to young Thy1-YFP mice (**Figure 3E**) (31,
263 32). ISRIB treatment significantly increased spine numbers when compared with age-
264 matched vehicle-treated mice (**Figure 3E**). Taken together these data demonstrate that
265 ISRIB administration improves both neuron structure and function in old mice.

266

267 *Age-induced inflammatory tone is reduced following ISRIB treatment.*

268

269 Because it is known that immune dysregulation in the brain increases with age (45) and
270 correlates with reduced cognitive performance in old animals (8, 9, 11, 20), we next
271 investigated immune parameters impacted by ISRIB administration in the old brain. To
272 this end, we first investigated glial cell activation (microglia and astrocytes) in
273 hippocampal sections from of old mice and ISRIB-treated old mice by fluorescent
274 microscopic imaging (during ISRIB administration, **Supplemental Figure 7**). We
275 measured, astrocyte and microglia reactivity as the percent area covered by GFAP and
276 Iba-1. In these analyses, we observed no differences between the old and ISRIB-
277 treated old animals (**Supplemental Figure 7B-G**).

278

279 Next, we performed quantitative PCR (qPCR) analyses on hippocampi from young, old,
280 and ISRIB-treated animals on samples taken at the same time point as in the
281 microscopic analysis (**Supplemental Figure 7A**). We measured a panel of
282 inflammatory markers, many of which are known to increase with age (45), with a
283 particular focus on IFN-related genes as this pathway is implicated in age-related
284 cognitive decline (20, 36). Indeed, we found that age increased expression of a number
285 of IFN response pathway genes, *Rtp4*, *Ifit1*, and *Gbp10* (**Figure 4A-C**). Importantly,
286 ISRIB administration reduced expression of *Rtp4*, *Ifit1*, and *Gbp10* to levels that
287 became indistinguishable from young animals (**Figure 4A-C**). Other inflammatory
288 makers were also increased with age (*Ccl2*, *Il6*) but not affected by ISRIB treatment,
289 whereas *Cd11b* was increased upon ISRIB administration alone (**Table 1**).

290
291 Using these same hippocampal extracts, we next measured T cell responses. Similar to
292 other reports (21, 46), we observed a significant increase in T cell marker mRNA
293 expression (*Cd3*) in the hippocampus of old compared to young mice (**Figure 4D**).
294 ISRIB treatment in the old mice reduced the expression of the T cell marker to a level
295 comparable to that observed in young mice (**Figure 4D**). The ISRIB-induced reduction
296 in T cell marker levels was not limited to the brain but extended to the peripheral blood
297 of old animals, with CD8⁺ T cell percentages reduced following ISRIB administration
298 (**Figure 4E**). By contrast, we observed no changes in CD4⁺ T cell levels (**Figure 4F**).

299
300 Given the broad and varied response of immune parameters in response to ISRIB
301 treatment, we next explored possible relationships between behavioral performance and

302 age-related inflammatory tone. T cell marker mRNA expression in the brain positively
303 correlated with cognitive performance: mice with lower T cell marker expression made
304 fewer errors prior to locating the escape platform during memory testing on Day 2
305 (**Figure 4G**). We also observed significant positive correlations when comparing
306 memory performance on day 2 (errors) with the mRNA levels of multiple IFN response
307 pathway genes (*Ifit1*, *Rtp4*, *Gbp10*, *Gbp5*, *Oasl1*) and additional inflammatory markers
308 (*Ccl2*, *Il6*) (**Figure 4G**). These data demonstrate that increased inflammatory marker
309 expression correspond with poorer cognitive performance, even when we did not
310 observed differences between the groups. These studies revealed that ISRIB treatment
311 impacts a broad number of immune parameters both in the periphery and in the brain
312 reducing the age-related inflammatory tone which strongly correlates with improved
313 cognition.

314

315 *ISRIB treatment resets age-related ISR activation*

316

317 Finally, we investigated the transcriptional expression of ISR mediators and neuronal
318 health markers in the hippocampal lysates used above. We did not detect differences in
319 *Gadd34*, *Pkr*, *Bdnf1*, and *Ophn1* mRNA levels with age or ISRIB treatment (**Table 1**).
320 Interestingly however, when analyzed as individual animals, we found a negative
321 correlation between *Gadd34* mRNA and cognitive performance: animals with less
322 *Gadd34* mRNA made more errors prior to locating the escape platform during memory
323 testing (**Figure 5A**). GADD34, the regulatory subunit of one of the two eIF2 α
324 phosphatases, acts in a feedback loop as a downstream target of ATF4 (47-49).

325 Induction of GADD34 leads to decreased phosphorylation of eIF2 which counteracts
326 ISR activation. Indeed, ISRIB treatment reduced p-eIF2 levels in total brain lysates
327 (**Figure 5B; Supplemental Figure 8**), suggesting that ISRIB may break a feedback
328 loop thereby resetting age-related ISR activation.

329

330

331 **CONCLUSION**

332 We provide evidence for a direct involvement of the ISR in age-related cognitive
333 decline. Temporary treatment with ISRIB causes down-regulation of ATF4 for at least
334 20 days. This “ISR reset” leads to improvement in spatial, working, and episodic
335 memory. At a cellular level the cognitive enhancement is paralleled by i) improved
336 intrinsic neuron excitability, ii) increased dendritic spine density, iii) reversal of age-
337 induced changes in IFN and T cell responses in the hippocampus and blood, and iv)
338 reversal of ISR activation. Thus, we identify broad-spectrum anatomical, cellular, and
339 functional changes caused by ISR activation in old animals. If these findings in mice
340 translate into human physiology, they offer hope and a tangible strategy to sustain
341 cognitive ability as we age.

342

343

344

345

346

347

348 **FIGURE AND TABLE LEGENDS**

349

350 **Figure 1. ISRIB resets the ISR in the brain of old mice.** (A) Experimental dosing
351 scheme: ISRIB treatment denoted by syringes (3 injections). (B) ISRIB treatment
352 reduced ATF4 protein levels chronically 18 days after ISRIB treatment was complete.
353 One-way ANOVA ($F = 18.8$, $p < 0.001$); with Tukey post-hoc analysis. (C) Modest age-
354 induced increases in p-GCN2 when comparing young and old male mice. One-way
355 ANOVA ($F = 6.6$, $p < 0.05$); with Tukey post-hoc analysis. (D, E) Age and ISRIB
356 administration did not impact p-PERK or p-PKR protein levels. Brain lysates of specific
357 protein levels listed normalized to actin. Young $n = 5$, Old = 3, Old + ISRIB = 3.
358 Individual animal values represented by dots; lines depict group mean \pm SEM. * $p <$
359 0.05 ; *** $p < 0.001$

360

361 **Figure 2. Inhibition of the ISR reverses age-induced decline in spatial, working**
362 **and episodic memory.** (A) Experimental Design: Old (~19 months) animals underwent
363 behavioral analysis in a radial arm water maze (RAWM) and a delayed matching to
364 place paradigm (DMP). ISRIB or vehicle administration (2.5 mg/kg intraperitoneal)
365 occurred daily during the learning phase of RAWM denoted by syringes (days 0-2). (B)
366 ISRIB treatment improved memory one week after administration in male rodents. One-
367 way ANOVA ($F = 5.3$, $p < 0.05$); with Tukey post-hoc analysis. Young $n = 10$; Old $n =$
368 25 ; Old + ISRIB $n = 21$. (C) Age-induced deficits in working and episodic learning and
369 memory restored weeks after ISRIB administration. Animals performed the DMP from
370 day 20 – 23. Average of all trials per group for each day. Day 20, 21 = 4 trials/day. Day
371 22,23 = 3 trials/day. Two-way repeated measures ANOVA reveals a significant
372 difference between groups $p < 0.01$ (denoted in figure legend) and time effect $p < 0.01$.
373 * $p < 0.05$, ** $p < 0.01$. Old $n = 18$; Old + ISRIB $n = 16$. Individual animal scores
374 represented by dots; lines depict group mean \pm SEM.

375

376

377 **Figure 3. ISRIB treatment alleviates age-associated changes in CA1 pyramidal**
378 **neuron function and structure.** (A) Left: Image of pipette patched onto CA1 neuron in
379 sagittal slice of hippocampus. Right: Representative traces from hippocampal CA1
380 pyramidal neurons from old animals treated with either vehicle (light blue) or ISRIB
381 (dark blue) or young animals treated with vehicle (orange) showing the response to a
382 current injection eliciting ~50Hz spiking activity. Spikes are truncated (dashed line), and
383 the AHP is visualized immediately following cessation of current injection (yellow
384 square) and quantified as the change in voltage from baseline (dotted line). (B) Age-
385 induced increases in AHP were measured when comparing young and old animals.
386 ISRIB treatment reversed increased AHP to levels indistinguishable from young
387 animals. Animals were injected with ISRIB (2.5 mg/kg) or vehicle intraperitoneal one
388 day prior to recordings. One-way ANOVA ($F = 4.461$, $p < 0.05$); with Tukey post-hoc
389 analysis. * $p < 0.05$. Each neuron is represented with a symbol; lines indicate the mean \pm
390 SEM (Neurons: Young males $n = 10$ (5 animals); Old males $n = 12$ (5 animals), Old +
391 ISRIB males $n = 19$ (7 animals) with 1-5 neurons recorded per animal. (C-E) Spine
392 density was quantified in the CA1 region of the dorsal hippocampus from young and old
393 Thy1-YFP-H mice. (C) Diagram of hippocampal region analyzed. SR = stratum

394 radiatum. (D) Representative images from Old and Old + ISRIB mice. (E) A decrease in
395 dendritic spine density was measured when comparing old mice to young mice. ISRIB
396 treatment significantly increased spine density levels of old mice when compared to
397 vehicle treated old mice. 63x magnification with a water immersion objective. Young
398 males n = 7 slides (2 animals); Old males + Vehicle n = 12 slides (3 mice); Old males +
399 ISRIB n = 17 slides (4 mice). Individual slide scores (relative to old mice) represented in
400 dots, lines depict group mean \pm SEM. One-way ANOVA (F = 18.57, p < 0.001) with
401 Tukey post-hoc analysis. **p < 0.01; ***p < 0.001.

402
403 **Figure 4. Age-induced inflammatory tone is reduced following ISRIB treatment.**
404 Inflammatory genes were investigated in the hippocampus of young and old mice by
405 qPCR analysis. (A-C) ISRIB administration reversed age-induced increases in *Rtp4*,
406 *Ifit1*, and *Gbp10*. (A) *Rtp4*, One-way ANOVA (F = 12.23, p < 0.001) with a Tukey-post
407 analysis. Young males n = 8; Old males n = 7; Old + ISRIB males n = 8. (B) *Ifit1*, One-
408 way ANOVA (F = 8.8; p < 0.01) with a Tukey-post analysis. Young males n = 8; Old
409 males n = 7; Old + ISRIB males n = 8. (C) *Gbp10*, One-way ANOVA (F = 4.2, p < 0.05)
410 with a Tukey-post analysis. Young males n = 8; Old males n = 7; Old + ISRIB males n =
411 7. (D) *Cd3* gene-expression (a marker for T cells) changes in the hippocampus of young
412 and old animals were measured by qPCR analysis. *Cd3* was significantly increased with
413 age. ISRIB administration returned *Cd3* expression levels to those comparable to young
414 animals. One-way ANOVA (F = 5.2; p < 0.05). Tukey-post hoc analysis. Young males n
415 = 8; Old males n = 7; Old + ISRIB males n = 8. (E, F) Peripheral T cell levels were
416 measured by flow cytometric analysis of whole blood. (E) ISRIB treatment reduced
417 CD8⁺ T cell percentages (of CD45⁺ cells) in the peripheral blood. Student t-test. Old
418 males n = 7; Old + ISRIB males n = 8. (F) CD4⁺ T cell percentages (of CD45⁺ cells)
419 were not impacted. Individual animal scores represented by dots; lines depict group
420 mean \pm SEM. (G) A significant positive correlation was measured between cognitive
421 performance on day 2 of the RAWM (errors) and multiple inflammatory markers (*Cd3*,
422 *Ifit1*, *Rtp4*, *Gbp10*, *Gbp5*, *Oasl1*, *Ccl2*, *Il-6*). Linear regression was measured by
423 Pearson R correlation, R value denoted with significance. *p < 0.05; **p < 0.01; ***p <
424 0.001.

425
426 **Figure 5. ISRIB treatment resets age-related ISR activation.** (A) A significant
427 negative correlation was measured between cognitive performance on day 2 of the
428 RAWM (errors) and *Gadd34* mRNA expression. Linear regression was measured by
429 Pearson R correlation, R value denoted with significance. (B) ISRIB treatment reduced
430 p-eIF2 α protein levels. Brain lysates of p-eIF2 α protein levels normalized to actin. Old
431 males n = 10; ISRIB males n = 10. Student's t-test. **p < 0.01. Data are means \pm SEM.

432
433
434 **Table 1. Impact of age and ISRIB on mRNA expression in the hippocampus.**
435 Inflammatory, ISR mediators and neuronal health targets were investigated by qPCR
436 analysis of hippocampal lysates after two ISRIB injections. Columns: (i) mRNA targets
437 (ii) Young group mean \pm SEM (iii) Old group mean \pm SEM (iv) Old + ISRIB group mean
438 \pm SEM (v) ANOVA F value (vi) Significant denotation between groups (vii) n/group.

439

440
441
442
443
444
445
446
447
448
449
450
451
452
453
454
455
456
457
458
459
460
461
462
463
464
465
466
467
468
469
470
471
472
473
474
475
476
477
478
479
480
481
482
483
484
485

Supplemental Figure 1. ISRIB downregulates ATF4 during administration. The impact of ISRIB on known ISR activation pathways was investigated by Western blot analysis of brain lysates after 3 ISRIB injections. **(A)** Raw western blot data. Each lane represents an individual animal brain extract. **(B)** ISRIB treatment reduced ATF4 protein levels during drug administration. Old males (7) and females (3): Old n = 10; Old + ISRIB n = 10. Student's t-test. *p < 0.05. Individual animal values represented by dots; lines depict group mean ± SEM.

Supplemental Figure 2. ISRIB down-regulates the ISR in the brain of old mice. The impact of ISRIB on known ISR kinases and activation pathways was investigated by Western blot analysis of brain lysates (raw Western blot data) at day 20. **(A)** ATF4 **(B)** p-GCN2, p-PKR, p-PERK. Each lane represents an individual animal brain extract.

Supplemental Figure 3. ISR inhibitors relieve age-induced deficits in spatial learning. RAWM was used to measure age-induced deficits in spatial learning. Animals ran 2 blocks (3 trials/block) on each learning day. **(A)** Old animals performed significantly worse than young animals. Two-way repeated measures ANOVA revealed a significant interaction (p < 0.001). Bonferroni post-hoc to determine differences at various blocks. Old males n = 19, Young males n = 10. *p < 0.05. **(B)** ISRIB or vehicle administration (2.5 mg/kg intraperitoneal) occurred days 0-2. Compared with the old group, ISRIB treated animals made significantly fewer errors over the course of learning. Two-way repeated measures ANOVA reveals a significant difference between groups p < 0.05. Old males n = 19; Old + ISRIB males n = 15. **(C)** No differences were measured between young +/- ISRIB administration. Two-way repeated measures ANOVA revealed no significant differences. Young males n = 10; Young males + ISRIB n = 10 **(D)** Cmp-003 (5 mg/kg intraperitoneal) administration occurred days 0-2. Old mice that received Cmp-003 performed significantly better than old mice that received vehicle. Two-way repeated measures ANOVA revealed a significant group (p < 0.01) and time effect (p < 0.05). Old males n = 9, Old males + Cmp-003 n = 9. **p < 0.01. Data are means ± SEM.

Supplemental Figure 4. ISRIB reduces age-induced memory deficits in female mice. RAWM was used to measure age-induced deficits in learning and memory. ISRIB treatment improved memory one week after administration in female rodents. Student t-test. Old female n = 12; Old female + ISRIB n = 11. * p < 0.05. Individual animal scores represented by dots, lines depict group mean and SEM.

Supplementary Figure 5. Age and ISRIB treatment do not modify other passive or active intrinsic membrane properties in CA1 pyramidal neurons. **(A)** Representative traces from CA1 pyramidal neurons showing the membrane potential response to a 250 pA current injection in neurons from old animals treated with either

486 vehicle (light blue) or ISRIB (dark blue) or young animals treated with vehicle (orange).
487 Quantification of the action potential (AP) including the half width (**B**), amplitude (**C**),
488 and threshold (**D**) did not show significant differences between CA1 pyramidal
489 recordings from old, old + ISRIB-treated, or young mice. Likewise, evaluation of the
490 maximum firing frequency (**E**) or how the frequency of spiking changes over time,
491 quantified by the adaptation index (**F**) or with current injection, quantified by the slope of
492 the relationship of firing frequency versus amplitude of current injection (F/I slope) (**G**)
493 was also not significantly different between groups. Finally, passive membrane
494 properties including the membrane time constant (τ) (**H**), membrane resistance (R_m)
495 (**I**), and the resting membrane potential (**J**) were not significantly altered by age or ISRIB
496 treatment. Each neuron is represented with a symbol; solid lines indicate the mean \pm
497 SEM. (One-way ANOVA for all comparisons; Neurons: and Young males $n = 12$ (5
498 animals); Old males $n = 15$ (5 animals), Old + ISRIB males $n = 22$ (7 animals) with 1-5
499 neurons recorded per animal.

500

501 **Supplemental Figure 6. Age and ISRIB treatment do not affect spontaneous**
502 **excitatory post-synaptic currents (sEPSC) in CA1 pyramidal neurons.** (**A**)
503 Representative whole cell voltage-clamp recordings showing sEPSCs from CA1
504 pyramidal neurons from old animals treated with either vehicle (light blue) or ISRIB
505 (dark blue) or young animals treated with vehicle (orange). Arrows denote synaptic
506 currents. (**B**) The sEPSC amplitude was not significantly difference between groups
507 (one-way ANOVA). (**C**) The sEPSC frequency was unchanged after ISRIB treatment or
508 compared to young mice (Kruskal-Wallis test). The median amplitude or frequency for
509 each neuron is represented with a symbol; solid lines indicate the mean \pm SEM.
510 (Neurons: Young males $n = 11$ (5 animals); Old males $n = 15$ (5 animals), Old + ISRIB
511 males $n = 18$ (7 animals) with 1-5 neurons recorded per animal.)

512

513 **Supplemental Figure 7. ISRIB administration does not impact glial cell activation.**
514 (**A**) ISRIB administration scheme. (**B-G**) Glial cell was quantified in the stratum radiatum
515 of the CA1 region of the dorsal hippocampus from old Thy1-YFP-H mice. GFAP was
516 used to measure astrocyte activity. Representative images for GFAP staining of (**B**) old
517 and (**C**) old + ISRIB mouse. (**D**) No differences in GFAP percent area were measured
518 when comparing old and old + ISRIB animals. Iba-1 was used to measure microglia
519 activity. Representative images for Iba-1 staining of (**E**) old and (**F**) old + ISRIB mouse.
520 (**G**) No differences in Iba-1 percent area were measured when comparing old and old +
521 ISRIB animals. 63x magnification with a water immersion objective. Old males $n = 12$ -
522 19 slides (3 mice); Old males + ISRIB $n = 18$ - 20 slides (4 mice). Individual slide scores
523 (relative to old mice) represented in dots, lines depict group mean \pm SEM.

524

525 **Supplemental Figure 8. ISRIB treatment breaks age-related ISR activation.** The
526 impact of ISRIB on p-eIF2 was investigated by Western blot analysis of brain lysates
527 after 3 ISRIB injections. Raw western blot data. Each lane represents an individual
528 animal brain extract.

529

530

531

532
533
534
535
536
537
538
539
540
541
542
543
544
545
546
547
548
549
550
551
552
553
554
555
556
557
558
559
560
561
562
563
564
565
566
567
568
569
570
571
572
573
574
575
576
577

METHODS

Animals. All experiments were conducted in accordance with National Institutes of Health (NIH) Guide for the Care and Use of Laboratory Animals and approved by the Institutional Animal Care and Use Committee of the University of California, San Francisco (Protocol 170302). Male and female C57B6/J wild-type (WT) mice were received from the National Institute of Aging. Thy-1-YFP-H (in C57 background) were bred and aged in house. Old animals started experimentation at ~19 months of age and young animals 3-6 months of age. Animal shipments were received at least one week prior to start of experimentation to allow animals to habituate the new surroundings. Mice were group housed in environmentally controlled conditions with reverse light cycle (12:12 h light:dark cycle at 21 ± 1 °C; ~50% humidity) and provided food and water ad libitum. Behavioral analysis was performed during the dark cycle.

Drug Administration. ISRIB solution was made by dissolving 5 mg ISRIB in 2.5 mLs dimethyl sulfoxide (DMSO) (PanReac AppliChem, 191954.1611). The solution was gently heated in a 40 °C water bath and vortexed every 30 s until the solution became clear. Next 1 mL of Tween 80 (Sigma Aldrich, P8074) was added, the solution was gently heated in a 40 °C water bath and vortexed every 30 s until the solution became clear. Next, 10 mL of polyethylene glycol 400 (PEG400) (PanReac AppliChem, 142436.1611) solution was added gently heated in a 40 °C water bath and vortexed every 30 s until the solution became clear. Finally, 36.5 mL of 5% dextrose (Hospira, RL-3040) was added. The solution was kept at room temperature throughout the experiment. Each solution was used for injections up to 7 day maximum. The vehicle solution consisted of the same chemical composition and concentration (DMSO, Tween 80, PEG400 and 5% dextrose). Stock ISRIB solution was at 0.1 mg/ml and injections were at 2.5 mg/kg. Each animal received an intraperitoneal injection of 2.5x their body weight.

Cmp-003 solution was made by dissolving Cmp-003 (donated by Praxis Biotech) in 50% PEG400 (PanReac AppliChem, 142436.1611) and 50% sterile water. The solution was gently heated in a 40 °C water bath and vortexed every 30 s until the solution became clear. Stock Cmp-003 solution was at 0.5 mg/ml and animal injections were at 5.0 mg/kg. Solution was used immediately and made fresh daily.

Behavioral assessment of cognitive functions. For all behavioral assays the experimenter(s) were blinded to therapeutic intervention. Prior to behavioral analysis animals were inspected for gross motor impairments. Animals were inspected for whisker loss, limb immobility (included grip strength) and eye occlusions. If animals displayed *any* of these impairments, they were excluded. Behavioral assessment was recorded and scored using a video tracking and analysis setup (Ethovision XT 8.5, Noldus Information Technology).

Radial Arm Water Maze.

578 The radial arm water maze (RAWM) was used to test spatial learning and memory in
579 rodents (27, 42). The pool is 118.5 cm in diameter with 8 arms, each 41 cm in length,
580 and an escape platform. The escape platform is slightly submerged below the water
581 level, so it is not visible to the animals. The pool was filled with water that was rendered
582 opaque by adding white paint (Crayola, 54–2128-053). Visual cues are placed around
583 the room such that they were visible to animals exploring the maze. Animals ran 6 trials
584 a day during learning and 3 trials during each memory probe. On both learning and
585 memory days there is a 10-minute inter-trial interval. Animals were trained for 2 days
586 and then tested on memory tests 24 hours and 8 days after training. During a trial,
587 animals were placed in a random arm that did not include the escape platform. Animals
588 were allowed 1 min to locate the escape platform. On successfully finding the platform,
589 animals remained there for 10 s before being returned to their warmed, holding cage.
590 On a failed trial, animals were guided to the escape platform and then returned to their
591 holding cage 10 s later. The escape platform location was the same, whereas the start
592 arm varied between trials.

593
594 Animals were injected (intraperitoneal) with either vehicle or ISRIB (2.5 mg/kg) starting
595 the day prior to behavior (**Figure 2A**) and after each of the final trials of the learning
596 days (day 1 and 2) for a total of three doses. No injections were given when memory
597 was tested on days 3 and 10. RAWM data were collected through a video tracking and
598 analysis setup (Ethovision XT 8.5, Noldus Information Technology). The program
599 automatically analyzed the number of entries into non-target arms made per trial. Every
600 three trials were averaged into a block to account for large variability in performance;
601 each learning day thus consisted of 2 blocks, whereas each memory test was one block
602 each. Importantly, in all animal cohorts tested (regardless of age or drug treatment)
603 learning was measured (Significant time effect observed in all Two-way repeated
604 measure ANOVA analysis when groups are analyzed independently).

605
606 *Delayed Matching to Place Barnes Maze.*

607 Beginning at day 20 animals were tested on DMP using a modified Barnes maze (27,
608 44). The maze consisted of a round table 112 cm in diameter with 40 escape holes
609 arranged in three concentric rings consisting of 8, 16, and 16 holes at 20, 35, and 50 cm
610 from the center of the maze, respectively. An escape tunnel was connected to one of
611 the outer holes. Visual cues were placed around the room such that they were visible to
612 animals on the table. Bright overhead lighting and a loud tone (2 KHz, 85 db) were used
613 as aversive stimuli to motivate animals to locate the escape tunnel. The assay was
614 performed for 4 days (days 20-23). The escape tunnel location was moved for each day
615 and animals ran four trials on the first two days and 3 trials on the last two days. During
616 a trial, animals were placed onto the center of the table covered by an opaque plastic
617 box so they were not exposed to the environment. After they had been placed on the
618 table for 10 s, the plastic box was removed and the tone started playing, marking the
619 start of the trial. Animals were given 90 s to explore the maze and locate the escape
620 tunnel. When the animals successfully located and entered the escape tunnel, the tone
621 was stopped. If the animals failed to find the escape tunnel after 90 s, they were guided
622 to the escape tunnel before the tone was stopped. Animals remained in the escape
623 tunnel for 10 s before being returned to their home cage. The maze was cleaned with

624 ethanol between each trial. A new escape tunnel was used for each trial. The
625 experimenter was blind to the treatment groups during the behavioral assay. Each trial
626 was recorded using a video tracking and analysis setup (Ethovision XT 8.5, Noldus
627 Information Technology) and the program automatically analyzed the amount of time
628 required to locate the escape tunnel. Animal improvement was calculated by Day 20
629 escape latency – Day 23 escape latency.

630

631 Tissue collection. All mice were lethally overdosed using a mixture of ketamine (10
632 mg/ml) and xylazine (1 mg/ml). Once animals were completely anesthetized, blood was
633 extracted by cardiac puncture and animals were perfused with 1X phosphate buffer
634 solution, pH 7.4 (Gibco, Big Cabin, OK, -70011-044) until the livers were clear (~1–2
635 min). For Western blot analysis following phosphate buffered solution (PBS), the whole
636 brain (regions dissected discussed below) was rapidly removed and snap frozen on dry
637 ice and stored at –80 °C until processing.

638 Western Blot Analysis. Animals received all 3 ISRIB injections and were terminated 20 h
639 after the third injection (as described above). Frozen brain lysates or hippocampi
640 isolates were then homogenized with a T 10 basic ULTRA-TURRAX (IKA) in ice-cold
641 buffer lysis (Cell Signaling 9803) and protease and phosphatase inhibitors (Roche).
642 Lysates were sonicated for 3 min and centrifuged at 13,000 rpm for 20 min at 4°C.
643 Protein concentration in supernatants was determined using BCA Protein Assay Kit
644 (Pierce). Equal amount of proteins was loaded on SDS-PAGE gels. Proteins were
645 transferred onto 0.2 µm PVDF membranes (BioRad) and probed with primary antibodies
646 diluted in Tris-buffered saline supplemented with 0.1% Tween 20 and 3% bovine serum
647 albumin.

648

649 ATF4 (11815) (Cell Signaling), p-GCN2 (Abcam Cat No ab-75836), p-PERK (Cell Signaling
650 Cat No 3179), p-PKR (Abcam Cat No ab-32036), and p-eIF2 (Cell Signaling, Cat No 3597)
651 and β-actin (Sigma-Aldrich) antibodies were used as primary antibodies. HRP-
652 conjugated secondary antibodies (Rockland) were employed to detect immune-reactive
653 bands using enhanced chemiluminescence (ECL Western Blotting Substrate, Pierce)
654 according to the manufacturer instructions. Quantification of protein bands was done by
655 densitometry using ImageJ software.

656

657 ATF4, p-GCN2, p-PERK, p-PKR and p-eIF2 levels were normalized to β-actin
658 expression and fold-change was calculated as the levels relative to the expression in
659 vehicle-treated derived samples, which corresponds to 1.

660

661 Electrophysiology.

662 Sagittal brain slices (250 µm) including the hippocampus were prepared from old mice
663 (~19 mo) treated with either vehicle or ISRIB or young mice (~3 mo), treated with
664 vehicle, 12-18 hours prior (n = 5, 7, and 5 per group respectively). Mice were
665 anesthetized with Euthasol (0.1 ml / 25 g, Virbac, Fort Worth, TX, NDC-051311-050-01),
666 and transcardially perfused with an ice-cold sucrose cutting solution containing (in mM):
667 210 sucrose, 1.25 NaH₂PO₄, 25 NaHCO₃, 2.5 KCl, 0.5 CaCl₂, 7 MgCl₂, 7 dextrose, 1.3
668 ascorbic acid, 3 sodium pyruvate (bubbled with 95% O₂ – 5% CO₂, pH 7.4) (see
669 **Supplemental Table 1** for reagent information). Mice were then decapitated and the

670 brain was isolated in the same sucrose solution and cut on a slicing vibratome (Leica,
671 VT1200S, Leica Microsystems, Wetzlar, Germany). Slices were incubated in a holding
672 solution (composed of (in mM): 125 NaCl, 2.5 KCl, 1.25 NaH₂PO₄, 25 NaHCO₃, 2
673 CaCl₂, 2 MgCl₂, 10 dextrose, 1.3 ascorbic acid, 3 sodium pyruvate, bubbled with 95%
674 O₂ – 5% CO₂, pH 7.4) at 36 °C for 30 min and then at room temperature for at least 30
675 min until recording.

676
677 Whole cell recordings were obtained from these slices in a submersion chamber with a
678 heated (32 – 34 °C) artificial cerebrospinal fluid (aCSF) containing (in mM): 125 NaCl, 3
679 KCl, 1.25 NaH₂PO₄, 25 NaHCO₃, 2 CaCl₂, 1 MgCl₂, 10 dextrose (bubbled with 95% O₂ -
680 5% CO₂, pH 7.4). Patch pipettes (3–6 MΩ) were manufactured from filamented
681 borosilicate glass capillaries (Sutter Instruments, Novato, CA, BF100-58-10) and filled
682 with an intracellular solution containing (in mM): 135 KGlucuronate, 5 KCl, 10 HEPES, 4
683 NaCl, 4 MgATP, 0.3 Na₃GTP, 7 2K-phosphocreatine, and 1-2% biocytin. CA1 pyramidal
684 neurons were identified using infrared microscopy with a 40x water-immersion objective
685 (Olympus, Burlingame, CA). Recordings were made using a Multiclamp 700B
686 (Molecular Devices, San Jose, CA) amplifier, which was connected to the computer with
687 a Digidata 1440A ADC (Molecular Devices, San Jose, CA), and recorded at a sampling
688 rate of 20 kHz with pClamp software (Molecular Devices, San Jose, CA). We did not
689 correct for the junction potential, but access resistance and pipette capacitance were
690 appropriately compensated before each recording.

691
692 The passive membrane and active action potential spiking characteristics were
693 assessed by injection of a series of hyperpolarizing and depolarizing current steps with
694 a duration of 250 ms from –250 pA to 700 nA (in increments of 50 pA). The resting
695 membrane potential was the measured voltage of the cell 5 min after obtaining whole
696 cell configuration without current injection. A holding current was then applied to
697 maintain the neuron at –67 +/- 2 mV before/after current injections. The input resistance
698 was determined from the steady-state voltage reached during the –50 pA current
699 injection. The membrane time constant was the time required to reach 63% of the
700 maximum change in voltage for the –50 pA current injection. Action potential parameters
701 including the half width, threshold, and amplitude were quantified from the first action
702 potential elicited. Action potential times were detected by recording the time at which
703 the positive slope of the membrane potential crossed 0 mV. From the action potential
704 times, the instantaneous frequency for each action potential was determined (1 / inter
705 spike interval). The maximum firing frequency was the highest frequency of firing
706 identified throughout all current injections. Action potential rate as a function of current
707 injection was examined by plotting the first instantaneous action potential frequency
708 versus current injection amplitude. The F/I slope was then determined from the best
709 linear fit of the positive values of this plot. The action potential or spike threshold was
710 defined as the voltage at which the third derivative of V (d³V/dt) was maximal just prior
711 to the action potential peak. The action potential (AP) amplitude was calculated by
712 measuring the voltage difference between the peak voltage of the action potential and
713 the spike threshold. The half-width of the action potential was determined as the
714 duration of the action potential at half the amplitude. The adaptation index of each cell
715 was the ratio of the last over the first instantaneous firing frequency, calculated at 250

716 pA above the current step that first elicited spiking. The afterhyperpolarization (AHP)
717 was calculated as the change in voltage from baseline (measured as the mean voltage
718 over a 100 ms interval 600 ms after termination of a current injection that first elicited at
719 least 12 spikes corresponding to a firing frequency of ~50 Hz) compared to immediately
720 after cessation of current injection (the minimum voltage reached in the first 175 ms
721 immediately after cessation of current injection). Cells were excluded from analysis if
722 excessive synaptic input was noted during recording of the mAHP or if the cell did not
723 fire at least 12 spikes during current injections.

724
725 To measure the spontaneous excitatory postsynaptic currents (sEPSCs), cells were
726 recorded in voltage clamp at a holding potential of -75 mV for 4 min, a holding potential
727 that should have little inhibitory components given the reversal potential of chloride with
728 these solutions. Analysis of sEPSCs was performed using a template matching
729 algorithm in ClampFit 10.7 (Molecular Devices, San Jose, CA). The template was
730 created using recordings from multiple pyramidal cells and included several hundred
731 synaptic events. Access resistance (Ra) was monitored during recordings, and
732 recordings were terminated if Ra exceeded 30 megaohms. Only stable recordings (< 50
733 pA baseline change) with a low baseline noise (< 8 pA root mean square) were
734 included. The first 250 synaptic events or all the events measured in the 4 min interval
735 from each cell were included for analysis.

736
737 Fluorescent spine imaging preparation. For fluorescent spine analysis, following PBS
738 animals were perfused with ice-cold 4% paraformaldehyde, pH 7.5 (PFA, Sigma Aldrich,
739 St. Louis, MO, 441244) and fixed for 4 - 24 h followed by sucrose (Fisher Science
740 Education, Nazareth, PA, S25590A) protection (15% to 30%). Brains were embedded
741 with 30% sucrose/ Optimal Cutting Temperature Compound (Tissue Tek, Radnor, PA,
742 4583) mixture on dry ice and stored at -80 °C. Brains were sectioned into 20 µm slides
743 using a Leica cryostat (Leica Microsystems, Wetzlar, Germany) and mounted on slides
744 (ThermoFisher Scientific, South San Francisco, CA). Slides were brought to room
745 temperature (20 °C) prior to use. Tissues were fixed using ProLong Gold (Invitrogen,
746 Carlsbad, CA, P36930) and a standard slide cover sealed with nail polish.

747 Spine density quantification. For spine density quantification, whole brains from young
748 and old male Thy1-YFP-H transgenic line were used. 3-6 images separated by 60-140
749 µm in the dorsal hippocampus were imaged per animal and used for dendritic spine
750 density analysis. 9.3 µm z-stack images were acquired on a Zeiss Laser-Scanning
751 Confocal microscope (Zeiss LSM 780 NLO FLIM) at the HDFCCC Laboratory for Cell
752 Analysis Shared Resource Facility. 63x magnification with a water immersion objective.
753 All protrusions from the dendrites were manually counted as spines regardless of
754 morphology. Two individuals (blinded to age and treatment) analyzed a total length of at
755 least 3200 µm of dendrites from each animal using NIH FIJI analysis software (v1.52n).
756 Individual dendritic spine was calculated as density per micron and graphed relative to
757 old mice.

758
759 qPCR Analysis. Hippocampus samples, of approximately the same size per animal
760 were process as previously described (50, 51). Relative gene expression was

761 determined using the 2- $\Delta\Delta C_t$ method and normalized using GAPDH. Primers used were
762 the following:

763
764 *Cd3*: Fw 5' TGACCTCATCGCAACTCTGCTC-3' Rev 5'
765 TCAGCAGTGCTTGAACCTCAGC-3'

766
767 *Ifit1*: Fw 5' CTGAGATGTCACTTCACATGGAA-3' Rev 5'
768 GTGCATCCCCAATGGGTTCT-3'

769
770 *Rtp4*: Fw 5' TGGGAGCAGACATTTCAAGAAC-3', Rev
771 5'ACCTGAGCAGAGGTCCAACCTT-3'

772 *Gbp10*: Fw 5' GGAGGCTCAAGAGAAAAGTCACA-3', Rev 5'
773 AAGGAAAGCCTTTTGATCCTTCAGC-3'

774
775 *Ccl2*: Fw 5' GCTGACCCCAAGAAGGAATG-3' Rev 5' GTGCTTGAGGTGGTTGTGGA-
776 3'

777
778 *Il1 β* : Fw 5' TGTAATGAAAGACGGCACACC-3' Rev 5' TCTTCTTTGGGTATTGCTTGG-
779 3'

780
781 *Tnfa*: Fw 5' TGCCTATGTCTCAGCCTCTTC-3' Rev 5' GAGGCCATTTGGGAACTTCT-
782 3'

783
784 *Il-6*: Fw 5' TACCACTTCACAAGTCGGAGGC-3' Rev 5'
785 CTGCAAGTGCATCATCGTTGTTC-3'

786
787 *Irf7*: Fw 5'- GAGACTGGCTATTGGGGGAG-3' Rev 5'- GACCGAAATGCTTCCAGGG-3'

788
789 *Ifitm3*: Fw 5'- CCCCCAACTACGAAAGAATCA-3' Rev 5'-
790 ACCATCTTCCGATCCCTAGAC-3'

791
792 *Isg15*: Fw 5'- GGTGTCCGTGACTAACTCCAT-3' Rev 5'-
793 TGGAAGGGTAAGACCGTCCT-3'

794
795 *Ifi204*: Fw 5'- AGCTGATTCTGGATTGGGCA-3' Rev 5'-
796 GTGATGTTTCTCCTGTTACTTCTGA-3'

797
798 *Eif2ak2 (Pkr)*: Fw 5'- CTGGTTCAGGTGTCACCAAAC-3' Rev 5'-
799 ACAACGCTAGAGGATGTTCCG-3'

800
801 *Cd11b*: Fw 5'- CTGAGACTGGAGGCAACCAT- 3' Rev 5'
802 GATATCTCCTTCGCGCAGAC-3'

803
804 *Il-10*: Fw 5'- GCCAAGCCTTATCGGAAATG- 3' Rev 5' CACCCAGGGGAATTCAAATGC
805 -3'
806

807 *Bdnf*: Fw 5'- GGCTGACACTTTTGAGCACGT - 3' Rev 5'
808 CTCCAAAGGCACTTGACTGCTG -3'

809

810 *Ophn1*: Fw 5'- CTTCCAGGACAGCCAACCATTG
811 - 3' Rev 5' CTTAGCACCTGGCTTCTGTTC -3'

812

813 *Gbs5*: Fw 5'- CTGAACTCAGATTTTGTGCAGGA - 3' Rev 5'
814 CATCGACATAAGTCAGCACCAG -3'

815

816 *Oas1*: Fw 5'- CAGGAGCTGTACGGCTTCC - 3' Rev 5'
817 CCTACCTTGAGTACCTTGAGCAC -3'

818

819 *Gadd34*: Fw 5'- GCGGCTCAGATTGTTCAAAGC - 3' Rev 5'
820 CCAGACAGCAAGGAAATGGACTG -3'

821

822 *Gapdh*: Fw 5' AAATGGTGAAGGTCGGTGTG-3' Rev 5' TGAAGGGGTCGTTGATGG-3'

823

824 Flow Cytometric Analysis. To assess circulating cell populations peripheral blood was
825 collected by cardiac puncture and transferred into an EDTA collection tube. Blood was
826 aliquoted into flow cytometry staining tubes and stained with surface antibodies for 30-
827 60 min at room temperature (52). Surface antibodies included anti-CD45 (FITC-
828 conjugated; BD Biosciences), Ly-6G (PE-conjugated; BD Biosciences), CD8 (PE-Cy7-
829 conjugated; BD Biosciences), CD4 (APC-conjugated; BD B), and CD11b (APC-Cy7; BD
830 Biosciences). Leukocyte subpopulations were identified as follows: Forward and side
831 scatter was used to exclude debris and doublet populations. Specific T- cell populations
832 were identified as follows: CD4 T-cell subsets were CD4+, CD45+, Ly-6G-, CD8-, CD11b-
833 . CD8 T-cell subsets were CD8+, CD45+, Ly-6G-, CD4-,CD11b-. After surface antibody
834 staining, red blood cells were lysed with RBC lysis (BD Biosciences). Cell population
835 gating occurred as previously described (52). (Data were collected on an LSRII (BD)
836 and analyzed with Flowjo™ software (v10, Tree Star Inc.).

837

838 Statistical Analysis. Results were analyzed using Prism software or IBM SPSS
839 Statistics. Individual animals. Individual animal scores represented by dots, lines depict
840 group mean and SEM. Student t-test, one-way ANOVA, two-way repeated measures
841 ANOVA and Pearson R correlations were used (individual statistical tool and post-hoc
842 analysis denoted in Figure Legends). p values of < 0.05 considered as significant.

843

844

845 **Supplemental Table 1. List of Electrophysiology Reagents.**

REAGENTS FOR PATCHING	Company	Product#
Sucrose	Sigma-Aldrich, St. Louis, MO	S5016
NaH ₂ PO ₄	Sigma-Aldrich, St. Louis, MO	S9638
NaHCO ₃	Sigma-Aldrich, St. Louis, MO	S6014
KCl	Sigma-Aldrich, St. Louis, MO	P9333
NaCl	Sigma-Aldrich, St. Louis, MO	S9888
CaCl ₂	Sigma-Aldrich, St. Louis, MO	223506
MgCl ₂	Sigma-Aldrich, St. Louis, MO	M9272
Dextrose	Sigma-Aldrich, St. Louis, MO	G5767
Ascorbic acid	Sigma-Aldrich, St. Louis, MO	A5960
Sodium pyruvate	Sigma-Aldrich, St. Louis, MO	P5280
Potassium gluconate	Sigma-Aldrich, St. Louis, MO	P1847
HEPES	Sigma-Aldrich, St. Louis, MO	H3375
MgATP	Sigma-Aldrich, St. Louis, MO	A9187
Na ₃ GTP	Sigma-Aldrich, St. Louis, MO	G8877
2K-phosphocreatine	Millipore, Burlington, MA	237911
Biocytin	Tocris, Bristol, UK	3349

846
847

848
849
850
851
852
853
854
855
856
857
858
859
860
861
862
863
864
865
866
867
868
869
870
871
872
873
874
875
876
877
878
879
880
881
882
883

ACKNOWLEDGEMENTS

This work was supported by the generous support of the Rogers Family (to S.R. and P.W.), the UCSF Weill Innovation Award (to S.R. and P.W.), the NIH/National Institute on Aging Grant R01AG056770 (to S.R.), the NRSA post-doctoral fellowship from the NIA F32AG054126 (to K.K), the National Institute for General Medicine (NIGMS) Initiative for Maximizing Student Development (R25GM056847) and the National Science Foundation (NSF) Graduate Fellowship Program (To E.S.F), the UCSF Clinical and National Center for Advanced Translational Sciences at NIH (UCSF-CTSI Grant Number TL1 TR001871) and the NIH/NINDS (K08NS114170) (To A.N), the Programa de Apoyo a Centros con Financiamiento Basal AFB 170004 (to S.B.). P.W. is an Investigator of the Howard Hughes Medical Institute.

We thank Dr. Vikaas Sohal for providing equipment for electrophysiological recordings and advice on analysis. We thank Dr. Spyros Darmanis and Rene Sit from the Chan Zuckerberg Biohub for their assistance with analysis.

The authors would like to thank Praxis Biotech LLC, San Francisco, CA for providing samples of Cmp-003, for use in experiments described in this publication.

Microscopic imaging was obtained at the HDFCCC Laboratory for Cell Analysis Shared Resource Facility which is funded through grants from NIH (P30CA082103 and S10 ODo21818-01).

CONFLICT OF INTEREST

SB is an employee of Praxis Biotech. SB, GU and LD work at Fundacion Ciencia & Vida and receive partial funding from Praxis Biotech. P.W. is an inventor on U.S. Patent 9708247 held by the Regents of the University of California that describes ISRIB and its analogs. Rights to the invention have been licensed by UCSF to Calico. P.W. is a consultant for Praxis Biotech LLC and Black Belt TX Limited. The authors declare no other competing interests.

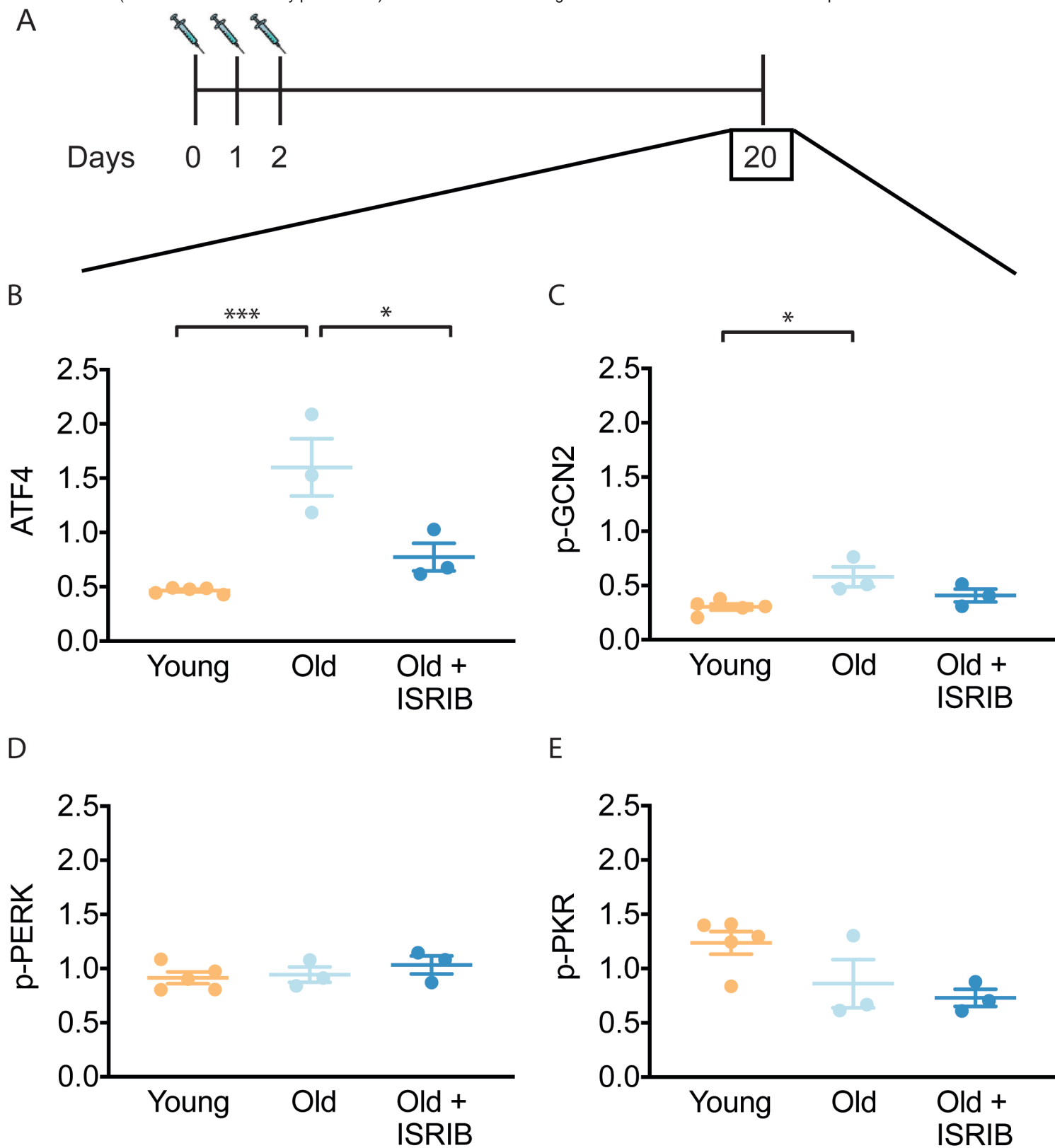
884
885
886
887
888
889
890
891
892
893
894
895
896
897
898
899
900
901
902
903
904
905
906
907
908
909
910
911
912
913
914
915
916
917
918
919
920
921
922
923
924
925
926
927
928
929

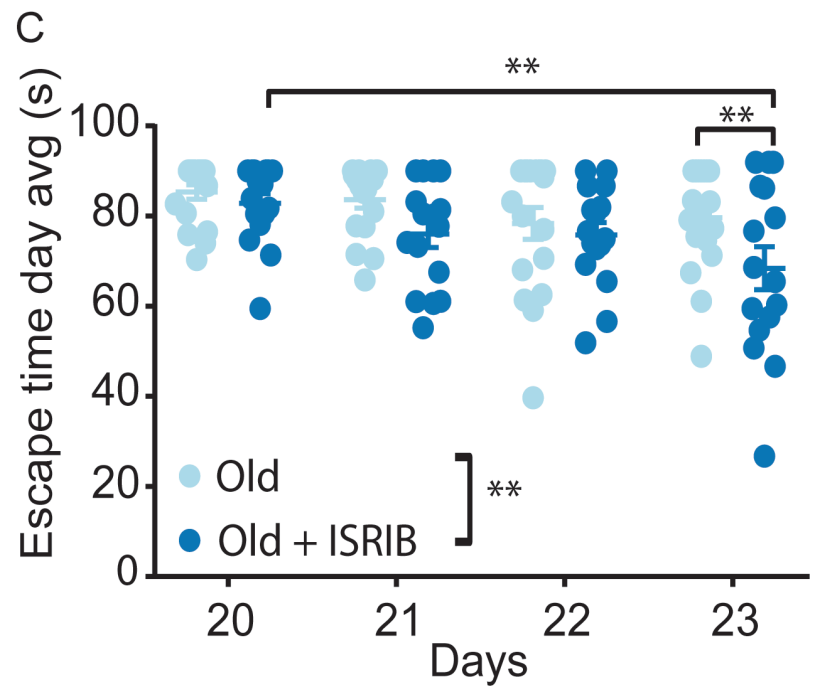
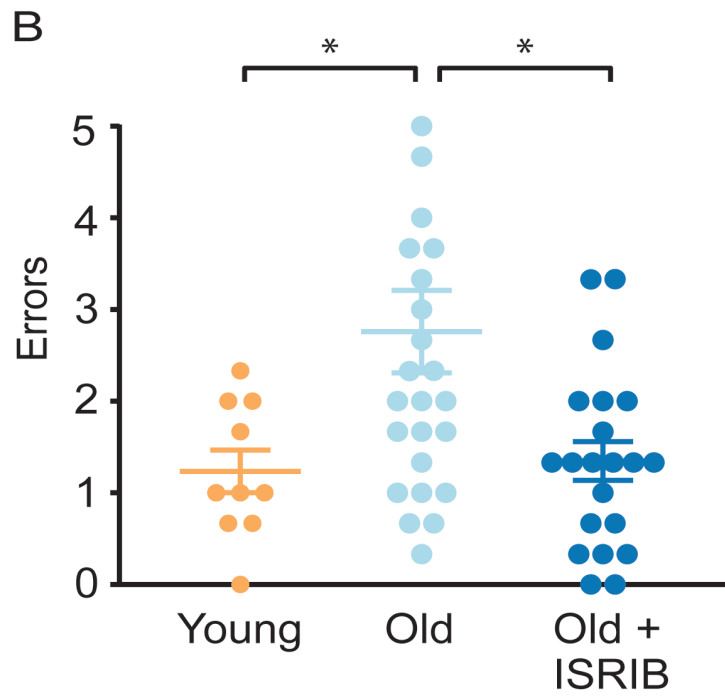
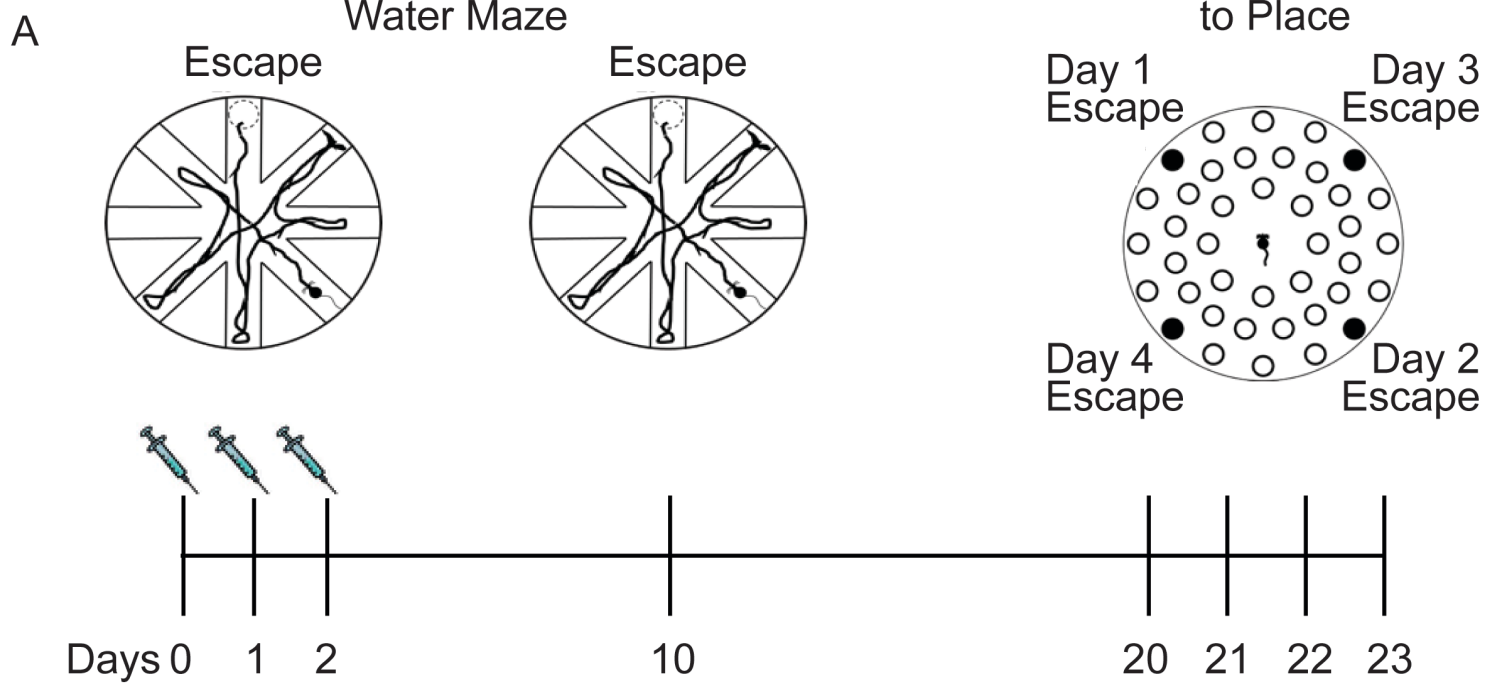
REFERENCES

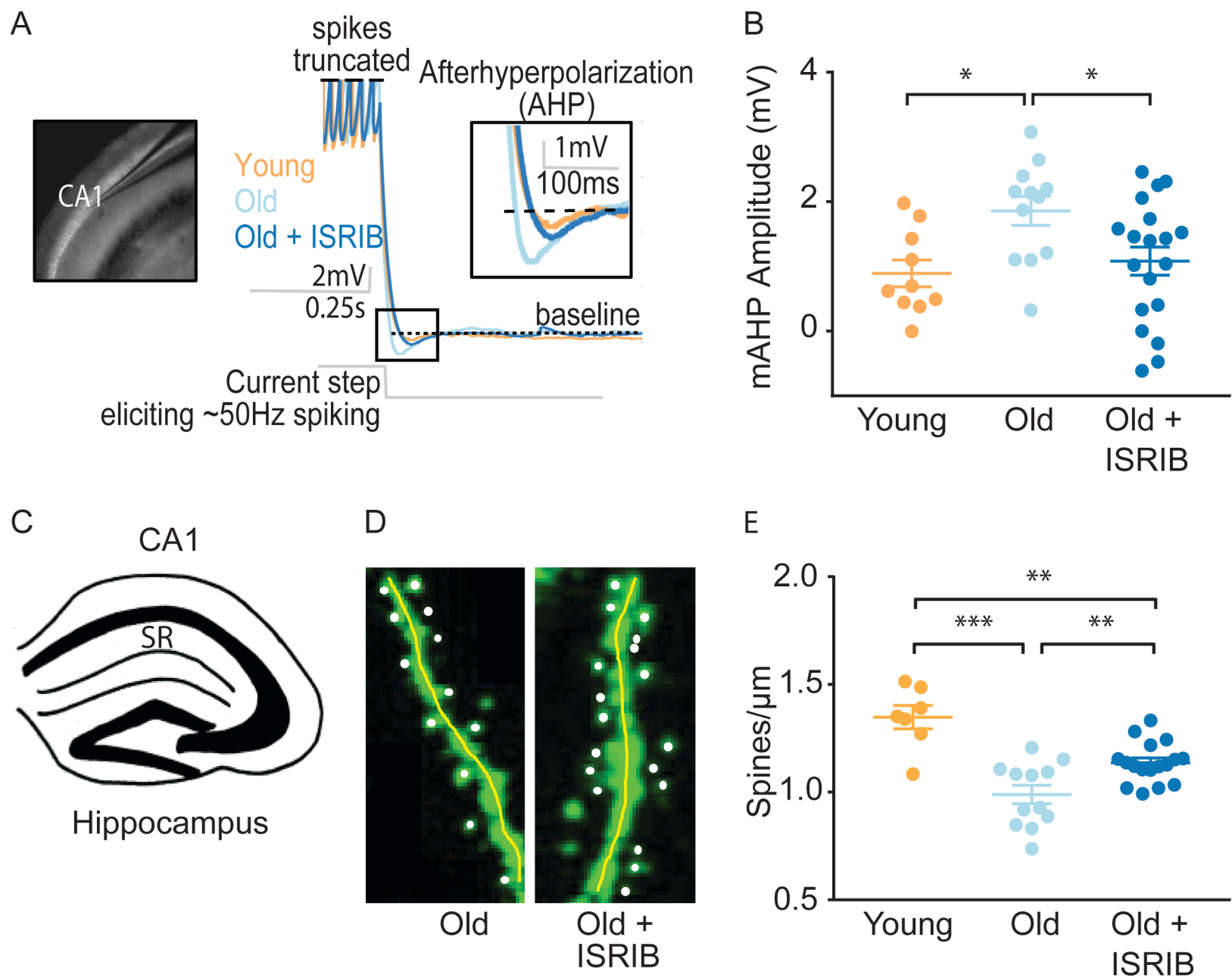
1. *Cognitive Aging. Progress in Understanding and Opportunities for Action* (2015).
2. S. L. Connelly, L. Hasher, R. T. Zacks, Age and reading: the impact of distraction. *Psychol Aging* **6**, 533-541 (1991).
3. N. D. Anderson, F. I. Craik, M. Naveh-Benjamin, The attentional demands of encoding and retrieval in younger and older adults: 1. Evidence from divided attention costs. *Psychol Aging* **13**, 405-423 (1998).
4. A. F. Kramer, S. Hahn, D. Gopher, Task coordination and aging: explorations of executive control processes in the task switching paradigm. *Acta Psychol (Amst)* **101**, 339-378 (1999).
5. N. J. Cepeda, A. F. Kramer, J. C. Gonzalez de Sather, Changes in executive control across the life span: examination of task-switching performance. *Dev Psychol* **37**, 715-730 (2001).
6. *An Aging Nation: The Older Population in the United States* (2014).
7. A. Chou, K. Krukowski, J. M. Morganti, L. K. Riparip, S. Rosi, Persistent Infiltration and Impaired Response of Peripherally-Derived Monocytes after Traumatic Brain Injury in the Aged Brain. *Int J Mol Sci* **19**, (2018).
8. H. Yousef *et al.*, Aged blood impairs hippocampal neural precursor activity and activates microglia via brain endothelial cell VCAM1. *Nat Med* **25**, 988-1000 (2019).
9. S. A. Villeda *et al.*, The ageing systemic milieu negatively regulates neurogenesis and cognitive function. *Nature* **477**, 90-94 (2011).
10. J. M. Castellano *et al.*, Human umbilical cord plasma proteins revitalize hippocampal function in aged mice. *Nature* **544**, 488-492 (2017).
11. S. A. Villeda *et al.*, Young blood reverses age-related impairments in cognitive function and synaptic plasticity in mice. *Nat Med* **20**, 659-663 (2014).
12. F. T. Cabral-Miranda, G. Martinez, G. Medinas, D. Gerakis, Y. Miedema, T. Duran-Aniotz, C. Ardiles, AO. Gonzalez, C. Sabusap, C. Bermedo-Garcia, F. Adamson, S. Vitangcol, K. Huerta, H. Zhang, X. Nakamura, T. Pablo Sardi, S. Lipton, SA. Kenedy, BK. Cárdenas, JC. Palacios, AG. Plate, L. Henriquez, JP. Hetz, C., Control of mammalian brain aging by the unfolded protein response (UPR). *Biorxiv*, (2020).
13. J. F. Disterhoft, M. M. Oh, Alterations in intrinsic neuronal excitability during normal aging. *Aging Cell* **6**, 327-336 (2007).
14. E. C. McKiernan, D. F. Marrone, CA1 pyramidal cells have diverse biophysical properties, affected by development, experience, and aging. *PeerJ* **5**, e3836 (2017).
15. M. M. Oh, F. A. Oliveira, J. F. Disterhoft, Learning and aging related changes in intrinsic neuronal excitability. *Front Aging Neurosci* **2**, 2 (2010).
16. V. Rizzo, J. Richman, S. V. Puthanveetil, Dissecting mechanisms of brain aging by studying the intrinsic excitability of neurons. *Front Aging Neurosci* **6**, 337 (2014).
17. L. A. Schimanski, C. A. Barnes, Neural Protein Synthesis during Aging: Effects on Plasticity and Memory. *Front Aging Neurosci* **2**, (2010).

- 930 18. V. Azzu, T. G. Valencak, Energy Metabolism and Ageing in the Mouse: A Mini-
931 Review. *Gerontology* **63**, 327-336 (2017).
- 932 19. C. Franceschi *et al.*, Inflamm-aging. An evolutionary perspective on
933 immunosenescence. *Ann N Y Acad Sci* **908**, 244-254 (2000).
- 934 20. K. Baruch *et al.*, Aging. Aging-induced type I interferon response at the choroid
935 plexus negatively affects brain function. *Science* **346**, 89-93 (2014).
- 936 21. B. W. Dulken *et al.*, Single-cell analysis reveals T cell infiltration in old neurogenic
937 niches. *Nature* **571**, 205-210 (2019).
- 938 22. J. B. Flexner, L. B. Flexner, E. Stellar, G. De La Haba, R. B. Roberts, Inhibition of
939 protein synthesis in brain and learning and memory following puromycin. *J*
940 *Neurochem* **9**, 595-605 (1962).
- 941 23. C. Lopez-Otin, M. A. Blasco, L. Partridge, M. Serrano, G. Kroemer, The
942 hallmarks of aging. *Cell* **153**, 1194-1217 (2013).
- 943 24. M. C. Ingvar, P. Maeder, L. Sokoloff, C. B. Smith, Effects of ageing on local rates
944 of cerebral protein synthesis in Sprague-Dawley rats. *Brain* **108 (Pt 1)**, 155-170
945 (1985).
- 946 25. C. B. Smith, Y. Sun, L. Sokoloff, Effects of aging on regional rates of cerebral
947 protein synthesis in the Sprague-Dawley rat: examination of the influence of
948 recycling of amino acids derived from protein degradation into the precursor pool.
949 *Neurochem Int* **27**, 407-416 (1995).
- 950 26. H. P. Harding *et al.*, An integrated stress response regulates amino acid
951 metabolism and resistance to oxidative stress. *Mol Cell* **11**, 619-633 (2003).
- 952 27. A. Chou *et al.*, Inhibition of the integrated stress response reverses cognitive
953 deficits after traumatic brain injury. *Proc Natl Acad Sci U S A* **114**, E6420-E6426
954 (2017).
- 955 28. K. Krukowski *et al.*, Integrated Stress Response Inhibitor Reverses Sex-
956 Dependent Behavioral and Cell-Specific Deficits after Mild Repetitive Head
957 Trauma. *J Neurotrauma*, (2020).
- 958 29. M. Costa-Mattioli, P. Walter, The integrated stress response: From mechanism to
959 disease. *Science* **368**, (2020).
- 960 30. C. C. Kaczorowski, J. F. Disterhoft, Memory deficits are associated with impaired
961 ability to modulate neuronal excitability in middle-aged mice. *Learn Mem* **16**, 362-
962 366 (2009).
- 963 31. O. von Bohlen und Halbach, C. Zacher, P. Gass, K. Unsicker, Age-related
964 alterations in hippocampal spines and deficiencies in spatial memory in mice. *J*
965 *Neurosci Res* **83**, 525-531 (2006).
- 966 32. B. Xu *et al.*, Loss of thin spines and small synapses contributes to defective
967 hippocampal function in aged mice. *Neurobiol Aging* **71**, 91-104 (2018).
- 968 33. E. B. Bloss *et al.*, Evidence for reduced experience-dependent dendritic spine
969 plasticity in the aging prefrontal cortex. *J Neurosci* **31**, 7831-7839 (2011).
- 970 34. N. Yasumatsu, M. Matsuzaki, T. Miyazaki, J. Noguchi, H. Kasai, Principles of
971 long-term dynamics of dendritic spines. *J Neurosci* **28**, 13592-13608 (2008).
- 972 35. U. I. Onat *et al.*, Intercepting the Lipid-Induced Integrated Stress Response
973 Reduces Atherosclerosis. *J Am Coll Cardiol* **73**, 1149-1169 (2019).
- 974 36. A. Deczkowska *et al.*, Mef2C restrains microglial inflammatory response and is
975 lost in brain ageing in an IFN-I-dependent manner. *Nat Commun* **8**, 717 (2017).

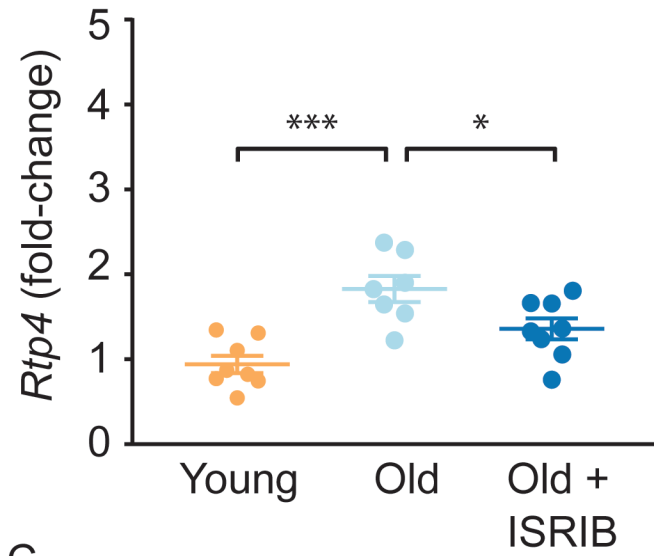
- 976 37. A. G. Hinnebusch, I. P. Ivanov, N. Sonenberg, Translational control by 5'-
977 untranslated regions of eukaryotic mRNAs. *Science* **352**, 1413-1416 (2016).
- 978 38. N. Sonenberg, A. G. Hinnebusch, Regulation of translation initiation in
979 eukaryotes: mechanisms and biological targets. *Cell* **136**, 731-745 (2009).
- 980 39. A. Chen *et al.*, Inducible enhancement of memory storage and synaptic plasticity
981 in transgenic mice expressing an inhibitor of ATF4 (CREB-2) and C/EBP
982 proteins. *Neuron* **39**, 655-669 (2003).
- 983 40. S. Pasini, C. Corona, J. Liu, L. A. Greene, M. L. Shelanski, Specific
984 downregulation of hippocampal ATF4 reveals a necessary role in synaptic
985 plasticity and memory. *Cell Rep* **11**, 183-191 (2015).
- 986 41. R. C. Wek, Role of eIF2alpha Kinases in Translational Control and Adaptation to
987 Cellular Stress. *Cold Spring Harb Perspect Biol* **10**, (2018).
- 988 42. J. Alamed, D. M. Wilcock, D. M. Diamond, M. N. Gordon, D. Morgan, Two-day
989 radial-arm water maze learning and memory task; robust resolution of amyloid-
990 related memory deficits in transgenic mice. *Nat Protoc* **1**, 1671-1679 (2006).
- 991 43. A. M. Horowitz *et al.*, Blood factors transfer beneficial effects of exercise on
992 neurogenesis and cognition to the aged brain. *Science* **369**, 167-173 (2020).
- 993 44. X. Feng, K. Krukowski, T. Jopson, S. Rosi, Delayed-matching-to-place Task in a
994 Dry Maze to Measure Spatial Working Memory in Mice. *Bio Protoc* **7**, (2017).
- 995 45. M. A. Oliveira Pisco A, Schaum N, Karkanas J, Neff NF, Darmanis S, Wyss-
996 Coray T, Quake SR, A Single Cell Transcriptomic Atlas Characterizes Aging
997 Tissues in the Mouse. *bioRxiv*, (2020).
- 998 46. D. Mrdjen *et al.*, High-Dimensional Single-Cell Mapping of Central Nervous
999 System Immune Cells Reveals Distinct Myeloid Subsets in Health, Aging, and
1000 Disease. *Immunity* **48**, 599 (2018).
- 1001 47. M. H. Brush, D. C. Weiser, S. Shenolikar, Growth arrest and DNA damage-
1002 inducible protein GADD34 targets protein phosphatase 1 alpha to the
1003 endoplasmic reticulum and promotes dephosphorylation of the alpha subunit of
1004 eukaryotic translation initiation factor 2. *Mol Cell Biol* **23**, 1292-1303 (2003).
- 1005 48. J. H. Connor, D. C. Weiser, S. Li, J. M. Hallenbeck, S. Shenolikar, Growth arrest
1006 and DNA damage-inducible protein GADD34 assembles a novel signaling
1007 complex containing protein phosphatase 1 and inhibitor 1. *Mol Cell Biol* **21**, 6841-
1008 6850 (2001).
- 1009 49. I. Novoa, H. Zeng, H. P. Harding, D. Ron, Feedback inhibition of the unfolded
1010 protein response by GADD34-mediated dephosphorylation of eIF2alpha. *J Cell*
1011 *Biol* **153**, 1011-1022 (2001).
- 1012 50. K. Krukowski *et al.*, Traumatic Brain Injury in Aged Mice Induces Chronic
1013 Microglia Activation, Synapse Loss, and Complement-Dependent Memory
1014 Deficits. *Int J Mol Sci* **19**, (2018).
- 1015 51. K. Krukowski *et al.*, Female mice are protected from space radiation-induced
1016 maladaptive responses. *Brain Behav Immun* **74**, 106-120 (2018).
- 1017 52. K. Krukowski, T. Jones, M. Campbell-Beachler, G. Nelson, S. Rosi, Peripheral T
1018 Cells as a Biomarker for Oxygen-Ion-Radiation-Induced Social Impairments.
1019 *Radiat Res* **190**, 186-193 (2018).
- 1020



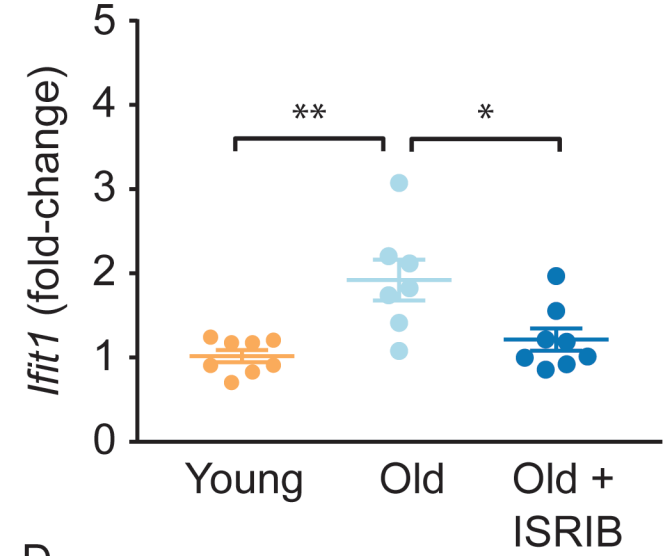




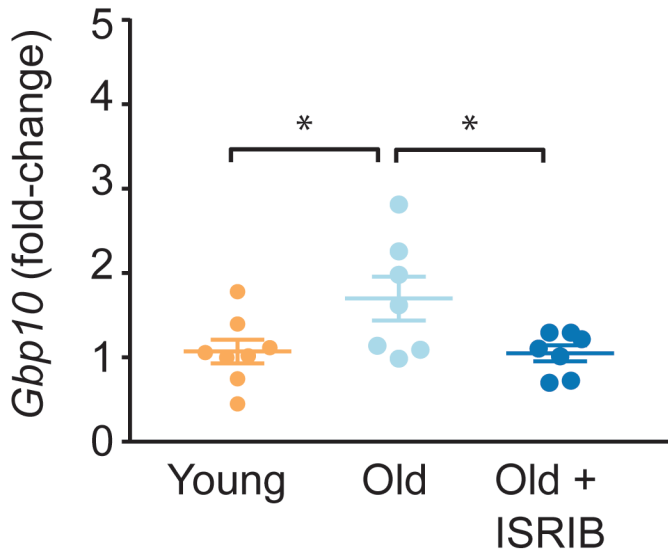
A



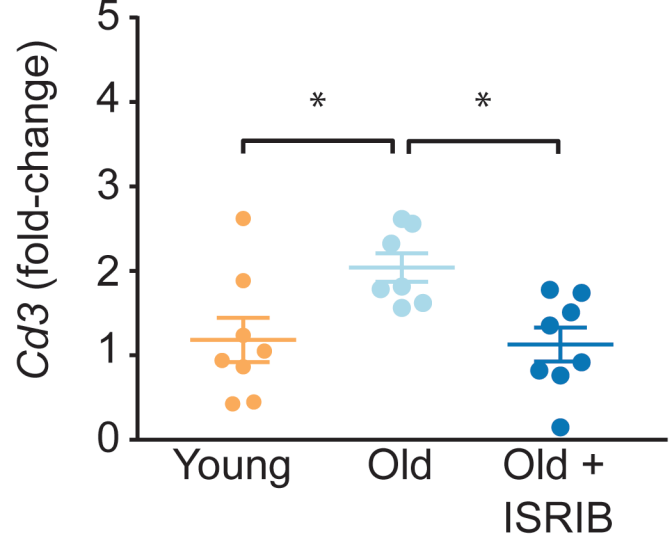
B



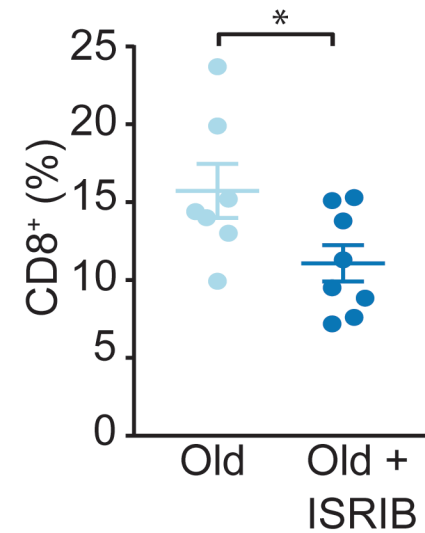
C



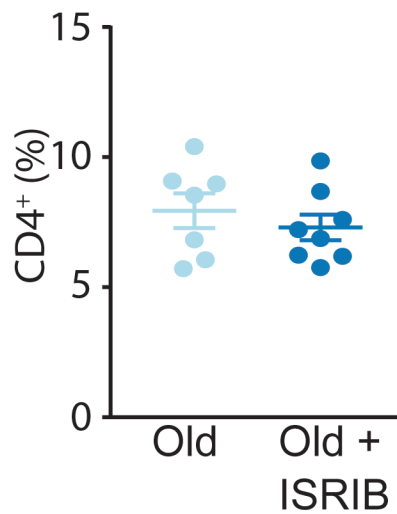
D



E



F



G

Errors	
<i>Cd3</i>	0.52**
<i>Ifit1</i>	0.56**
<i>Rtp4</i>	0.55**
<i>Gpb10</i>	0.54**
<i>Gbs5</i>	0.50*
<i>Oasl1</i>	0.47*
<i>Ccl2</i>	0.55**
<i>Il-6</i>	0.58**

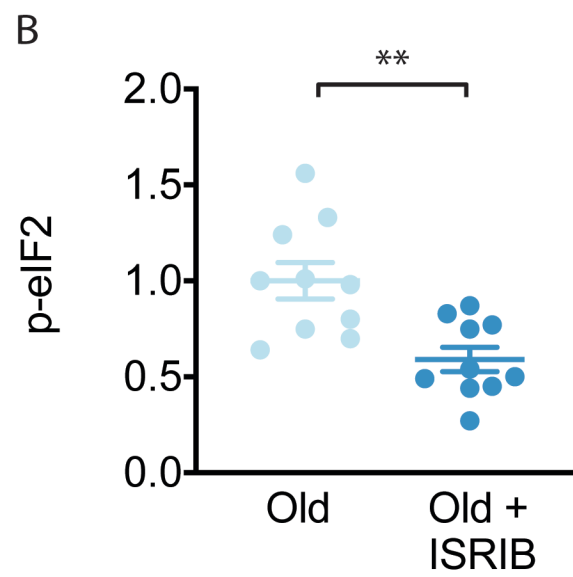
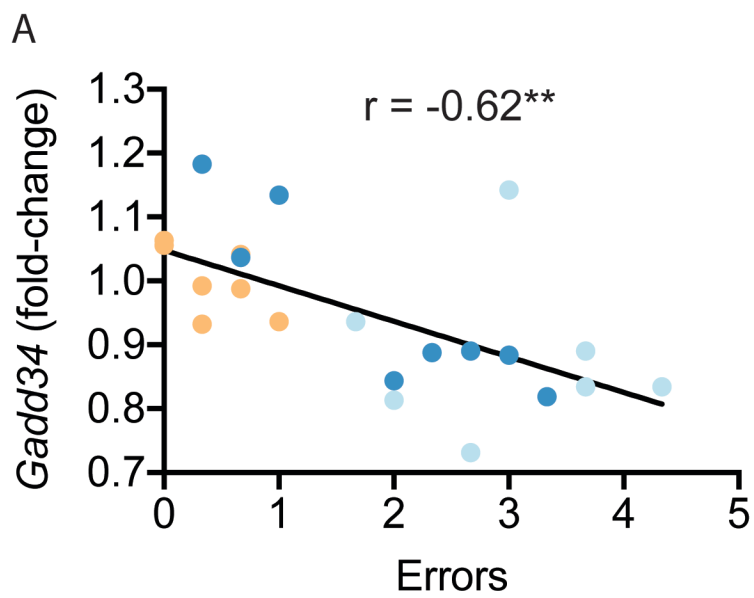


Table 1. Impact of age and ISRIB on mRNA expression in the hippocampus

TARGET	Young	Old	Old + ISRIB	ANOVA	Btw Groups	n: Yg/Old/Old + ISRIB
<i>Ccl2</i>	1.0 ± 0.1	2.3 ± 0.4	1.6 ± 0.1	F = 5.6*	Yg v Old**	8/7/7
<i>Cd11b</i>	1.0 ± 0.0	1.0 ± 0.0	1.2 ± 0.0	F = 6.6**	Yg v Old + ISRIB**	8/7/8
<i>Il1-β</i>	1.1 ± 0.1	1.4 ± 0.1	1.7 ± 0.1	F = 3.6*	Old v Old + ISRIB*	8/7/8
<i>Tnfα</i>	1.0 ± 0.1	1.6 ± 0.3	2.1 ± 0.4	F = 2.7		7/7/8
<i>Il-6</i>	1.1 ± 0.2	1.8 ± 0.1	1.8 ± 0.2	F = 4.1*	Yg v Old*	8/7/8
<i>Il-10</i>	1.0 ± 0.1	1.4 ± 0.2	1.5 ± 0.2	F = 1.1		7/7/7
<i>Irf7</i>	1.0 ± 0.1	1.4 ± 0.1	1.2 ± 0.1	F = 1.5		8/7/8
<i>Ifitm3</i>	1.0 ± 0.0	1.2 ± 0.1	1.0 ± 0.0	F = 0.8		8/7/8
<i>Isg15</i>	1.0 ± 0.0	1.3 ± 0.1	1.2 ± 0.0	F = 2.0		8/7/7
<i>Ifi204</i>	1.1 ± 0.2	1.4 ± 0.2	1.5 ± 0.1	F = 1.2		6/7/7
<i>Gbp5</i>	1.0 ± 0.0	1.2 ± 0.1	1.1 ± 0.0	F = 2.6		8/7/8
<i>Oasl1</i>	1.0 ± 0.0	1.8 ± 0.3	0.9 ± 0.1	F = 4.9*	Yg v Old*; Old v Old + ISRIB*	8/7/8
<i>Ophn1</i>	1.0 ± 0.0	0.9 ± 0.0	1.1 ± 0.0	F = 1.8		8/7/8
<i>Bdnf</i>	1.0 ± 0.0	0.9 ± 0.0	1.0 ± 0.0	F = 2.7		8/7/8
<i>Gadd34</i>	1.0 ± 0.0	0.8 ± 0.0	0.9 ± 0.0	F = 1.8		7/7/8
<i>Pkr</i>	1.0 ± 0.0	1.0 ± 0.0	1.1 ± 0.0	F = 1.0		8/7/8